

Review of recent results on heavy-ion physics and astroparticle physics in ALICE at the LHC

Héctor Bello and Arturo Fernández

Facultad de Ciencias Físico Matemáticas BUAP, 1152, Puebla, México.

Antonio Ortiz

Instituto de Ciencias Nucleares, UNAM, Ciudad de México, 04510, México

E-mail: antonio.ortiz@nucleares.unam.mx

Abstract.

In this work we present a summary of the most relevant results on heavy-ion and astroparticle physics in ALICE. The summary includes a brief overview of the current status on the characterization of the hot and dense QCD medium created in the heavy-ion collisions produced at the LHC, as well as the intriguing finding of collective-like phenomena in small collision systems.

1. Introduction

ALICE (A Large Ion Collider Experiment [1]) is a dedicated heavy-ion detector to exploit the unique physics potential of nucleus-nucleus interactions at the Large Hadron Collider (LHC) energies. The main goal of the detector is to study the physics of strongly interacting matter at extreme energy densities, where we have evidence that a new phase of matter, the quark-gluon plasma (QGP), is formed [2, 3, 4, 5]. Although several important measurements have been carried out by the LHC high energy physics experiments (CMS, ATLAS and LHCb), the present work focuses on results from ALICE and it is based on a recent review on heavy-ion physics at the LHC [6]. In this paper, we discuss the discovery of QGP-like phenomena in small collision systems, proton-proton (pp) and proton-lead (p-Pb) collisions. And also, we briefly discuss other contributions of ALICE in astroparticle physics.

2. The ALICE apparatus

Particle identification (PID) is an important tool to study the hot and dense matter created in heavy-ion collisions. Therefore, ALICE [7] is an experiment specialized in PID from low (≈ 0.15 GeV/ c) up to high (20 GeV/ c) transverse momenta. The central barrel of ALICE is placed inside a large solenoidal magnet which provides a magnetic field of 0.5 T. It is dedicated to detect hadrons, electrons, and photons produced at mid-pseudorapidity, $|\eta| < 0.8$. It comprises an Inner Tracking System (ITS) of high-resolution silicon detectors, a cylindrical Time-Projection Chamber (TPC), and particle identification arrays of Transition-Radiation Detectors (TRD) and of Time-Of-Flight (TOF) counters. Additional central subsystems, not-covering full azimuth, are a ring-imaging Cherenkov detector for High-Momentum Particle IDentification (HMPID), and

two electromagnetic calorimeters: a high-resolution PHOTon Spectrometer (PHOS) and a larger-acceptance ElectroMagnetic Calorimeter (EMCal). The muon arm detects muons emitted within $2.5 < \eta < 4$ and consists of a complex arrangement of absorbers, a dipole magnet, five pairs of tracking chambers, and two trigger stations. Several smaller detectors (VZERO, TZERO, FMD, ZDC, and PMD) for triggering, multiplicity measurements and centrality determination are installed in the forward region. On the three upper faces of the octagonal yoke of the solenoid, a dedicated cosmic ray detector (ACORDE [8]) is placed, which is made of 60 scintillator modules, covering 10% of solenoid upper faces. This subsystem produces a cosmic ray trigger signal when a single module fires (single muon cosmic ray event) or when more than two modules are activated by a cosmic ray shower.

3. Characterization of QGP

3.1. Soft probes

To learn about the early stage of the system, low transverse momentum ($p_T < 2.2 \text{ GeV}/c$) direct photons are studied. A temperature $T = 297 \pm 12^{\text{stat}} \pm 41^{\text{syst}}$ MeV has been measured for the 0-20% Pb–Pb collisions at $\sqrt{s_{\text{NN}}} = 2.76 \text{ TeV}$ [9]. Hence, the system at the LHC is hotter than that produced at RHIC, where an early temperature of $239 \pm 25^{\text{stat}} \pm 7^{\text{syst}}$ MeV was measured for the same centrality class in Au–Au collisions [10]. It is worth noticing that such temperatures are already above the one predicted to achieve the QCD phase transition [11]. In addition, the average multiplicity per number of participant is twice that measured at RHIC [12].

The system expands and cools down, then, the inelastic interactions cease and the yields of particles reach fixed values. This is the stage of the so-called chemical freeze-out which is studied using the yields of identified hadrons. Within 20% particle ratios, e.g., the proton yield normalized to that of pions, are described by thermal models with a common chemical freeze-out temperature of $T_{\text{ch}} \approx 156 \text{ MeV}$ [13]. However, large deviations are observed for protons and K^{*0} ; for the latter, this is not a surprise since its mean lifetime is smaller than that of the fireball ($\approx 10 \text{ fm}/c$) [14], and therefore the resonance yield may deviate from the expected values due to hadronic processes like re-scattering and regeneration [15].

On the other hand, the measurement of the spatial extent at decoupling time is obtained using intensity interferometry, a technique which exploits the Bose-Einstein enhancement of identical bosons emitted close by in phase space. This approach is known as Hanbury Brown-Twiss analysis (HBT) [16]. Using identical charged pions ALICE has measured a homogeneity volume of $\approx 300 \text{ fm}^3$ (two times that reported at RHIC) and a decoupling time of $\approx 10 \text{ fm}/c$ [14].

The transverse momentum distributions of identified hadrons contain valuable information about the collective expansion of the system ($p_T \lesssim 2 \text{ GeV}/c$), the presence of new hadronization mechanisms like quark recombination ($2 \lesssim p_T \lesssim 8 \text{ GeV}/c$) [17] and, at larger transverse momenta, the possible modification of the fragmentation due to the medium [18, 19]. ALICE has reported the transverse momentum spectra of charged pions, kaons and (anti)protons as a function of the collision centrality in broad transverse momenta intervals [20, 21, 22].

Figure 1 shows that for central Pb–Pb collisions the low p_T parts ($< 2 \text{ GeV}/c$) of the spectra are well described by hydrodynamic models (within 20%), except the low p_T ($< 1 \text{ GeV}/c$) proton yield [23, 24, 25, 26]. Models which best describe the data include hadronic rescattering with non-negligible antibaryon annihilation [25, 26]. The description of the results by hydrodynamic models is only observed in 0-40% Pb–Pb collisions, results for more peripheral collisions disagree with such prediction. This behavior has been recently studied for the average p_T in different colliding systems [27].

The analysis of the spectral shapes of the p_T distributions can be done using a blast-wave fit [28], which allows the extraction of the parameters related with the temperature at the kinetic freeze-out (T_{kin}) and the average transverse expansion velocity ($\langle \beta_T \rangle$). At the LHC, the radial flow in the most central collisions is found to be $\approx 10\%$ higher than at RHIC, while the kinetic

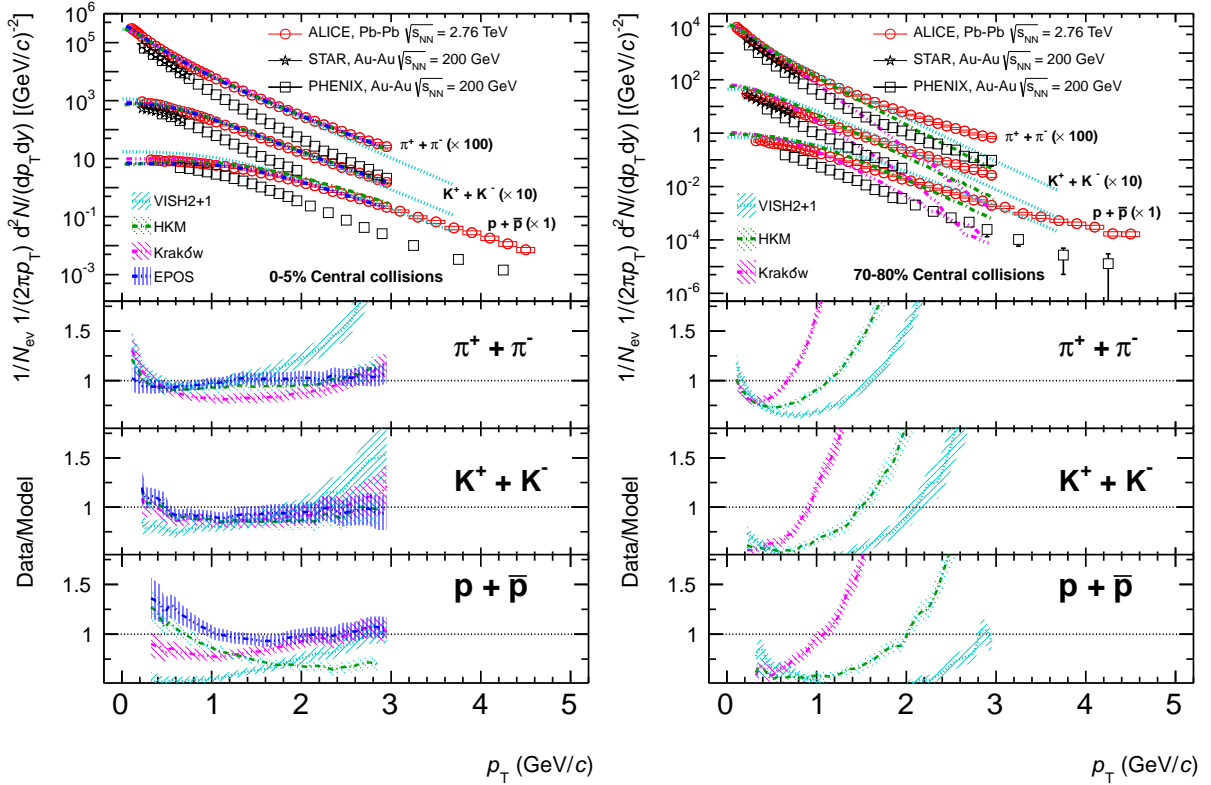


Figure 1. (Color online) Transverse momentum spectra of charged pions, kaons, and (anti)protons measured in central (left) and peripheral (right) Pb–Pb collisions at $\sqrt{s_{\text{NN}}} = 2.76$ TeV. The systematic and statistical uncertainties are plotted as color boxes and vertical error bars, respectively.

freeze-out temperature was found to be close to that measured at the RHIC, $T_{\text{kin}} = 95$ MeV [20]. From the study of the low p_{T} particle production we conclude that at the LHC the created system is larger, hotter and longer-lived than that produced at RHIC.

The intermediate p_{T} is studied with the particle ratios as a function of p_{T} [22]. For central heavy-ion collisions, Fig. 2 shows a comparison of particle ratios with results from STAR and PHENIX at the RHIC measured in Au–Au collision at $\sqrt{s_{\text{NN}}} = 200$ GeV. The proton-to-pion peak at the LHC is approximately 20% larger than at the RHIC, which is consistent with an increased average radial flow velocity. Interestingly, in ALICE we also observe a peak in the kaon-to-pion ratio supporting the idea of a strong radial flow. To check the effect of radial flow the shapes of the p_{T} distributions of ϕ -meson and protons are compared. The results indicate that for central Pb–Pb collisions the shapes of the proton-to-pion and ϕ -to-pion ratios are the same. On the other hand, for $p_{\text{T}} < 4$ GeV/c, the ϕ -meson yield normalized to that of protons becomes flat going from the most peripheral to the most central Pb–Pb collisions. This suggests that the mass, and not the number of quark constituents, determines the spectral shape in central Pb–Pb collisions. This is in a good agreement with the hydrodynamical interpretation. Recently, it has been shown that the spectral shapes, studied with the average p_{T} , exhibit a scaling with the hadron mass (number of constituent quarks) only in the 0-40% (40-90%) Pb–Pb collisions [27].

Using the scalar product method, the elliptic flow for identified hadrons has been

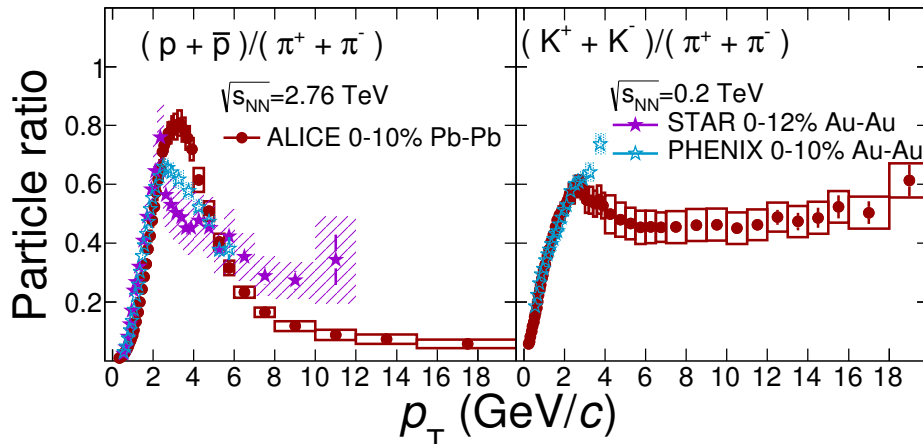


Figure 2. (Color online) ALICE (circles) results from $\sqrt{s_{\text{NN}}} = 2.76$ TeV Pb–Pb collisions compared with STAR and PHENIX results for $\sqrt{s_{\text{NN}}} = 200$ GeV Au–Au collisions. Left panel: the proton-to-pion ratio. Right panel: the kaon-to-pion ratio.

measured [29] over a broad p_T range. Going from central to semi-peripheral Pb–Pb collisions, the second order Fourier coefficient (v_2) increases as expected due to the eccentricity increase. For p_T below 2 GeV/ c a mass ordering is observed indicating the interplay between elliptic and radial flow. For higher p_T , the hadron- v_2 seems to be grouped into baryons and mesons, the exception is the v_2 of ϕ -mesons, which for central Pb–Pb collisions follows that for baryons. This observation indicates that the behavior of v_2 is driven by the hadron mass and not by the number of constituent quarks. ALICE has also reported the violation of the scaling of v_2 with the number of constituent quarks, such a observation is also against the scenario with quark recombination/coalescence.

3.2. Jet studies

The amount of suppression of inclusive particle production relative to pp collisions can be quantified with the nuclear modification factor, R_{AA} , defined as

$$R_{\text{AA}}(p_T) = \frac{1}{\langle T_{\text{AA}} \rangle} \frac{d^2 N^{\text{AA}}/dydp_T}{d^2 \sigma^{\text{pp}}/dydp_T} \quad (1)$$

where N^{AA} (σ^{pp}) is the yield (cross section) measured in AA (pp) collisions; and $\langle T_{\text{AA}} \rangle$ is the nuclear overlap function [30].

Figure 3 shows R_{AA} of full jets with $R = 0.2$ – 0.3 in central Pb–Pb collisions at $\sqrt{s_{\text{NN}}} = 2.76$ TeV. The data exhibit a strong suppression of the jet production relative to pp collisions [31]. Comparing the nuclear modification factor of charged jets to that of charged particles at large p_T one can see that the amount of the suppression is similar although the underlying parton p_T scale is different for inclusive particles and jets.

In order to study details of path-length dependence of energy loss, ALICE performed studies of elliptic anisotropy of inclusive charged jets [32] and semi-inclusive distributions of recoil jets [33] which complement and further extend earlier studies of elliptic anisotropies of inclusive high- p_T particles and modification of away-side di-hadron correlations [34]. For collisional energy loss, the path length dependence is expected to be linearly proportional to the length traversed by the parton in medium, while for radiative energy loss, where in addition interference effects

play a role, the dependence can be quadratic. In AdS/CFT class of models an even stronger dependence on path length traversed is predicted.

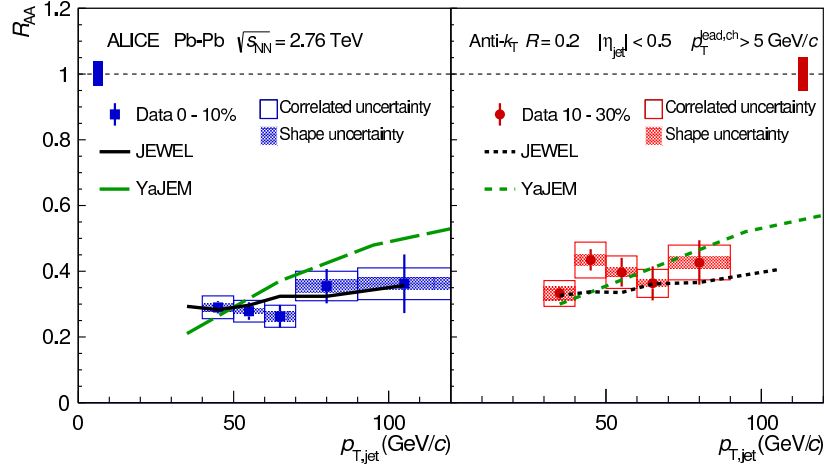


Figure 3. (Color online) Nuclear modification factor of full jets with $R = 0.2$ and p_T leading bias of $5 \text{ GeV}/c$ in central Pb–Pb collisions [35].

In Figure 4 the measurement of elliptic anisotropy v_2 for charged jets with the resolution parameter $R = 0.2$ is shown in central and semi-central Pb–Pb collisions. The data show significant positive v_2 value in semi-central Pb–Pb collisions pointing to the path length dependence of jet suppression. In central collisions the current uncertainties on the measurement do not allow to draw a definite conclusion, although the v_2 magnitude is also positive. These data are also compared to v_2 for full jets measured by ATLAS [36] and inclusive charged particles [37, 38]. Although these measurements cannot be directly compared quantitatively due to different p_T scales and centrality selections, qualitatively they agree and provide a clear evidence of path-length dependent parton energy loss.

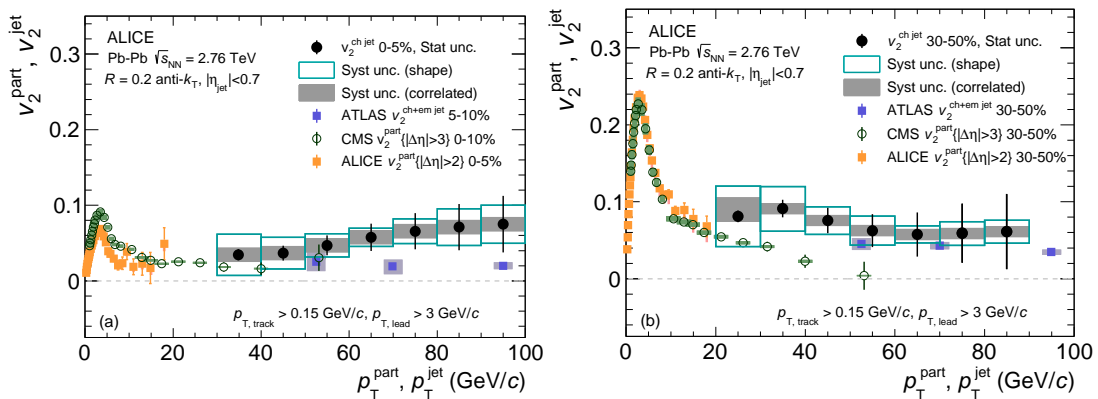


Figure 4. (Color online) Elliptic anisotropy (v_2) of inclusive charged particles and charged jets with the resolution parameter $R = 0.2$ in central (left) and semicentral (right) Pb–Pb collisions at $\sqrt{s_{NN}} = 2.76 \text{ TeV}$ measured by ALICE [32]. The data are compared with charged particle v_2 anisotropies measured by ALICE [37] and CMS [38] and calorimetric jets with $R = 0.2$ measured by ATLAS [36].

3.3. Open heavy flavour and quarkonia production

The nuclear modification factors of D mesons [39, 40] and electrons from heavy flavour decays [41] at mid-rapidity and of muons from heavy flavour decays at forward rapidity have been measured with ALICE. The results show a strong reduction of the yields (relative to pp) at large transverse momenta ($p_T \geq 5 \text{ GeV}/c$) in the most central collisions. Figure 5 (left) shows that, within uncertainties and in the measured p_T interval, the D meson nuclear modification factor is similar to that of charged pions and inclusive charged particles. It should be noted that the R_{AA} of D mesons and pions is also sensitive to the shape of the parton momentum distribution and their fragmentation functions. Model calculations including those effects and a colour-charge hierarchy in parton energy loss are able to describe the measurements [42].

In Fig. 5 (right), R_{AA}^D as a function of the average number of participant nucleons [43] is shown. This measurement is compared with results from the CMS collaboration of non-prompt J/ψ [44] and theoretical predictions [45, 46]. For D mesons, a smaller suppression in peripheral than in central collisions is observed. A larger suppression in central collisions is seen for D mesons than for non-prompt J/ψ , indicating a different energy loss for charm and beauty quarks. This observation is supported by predictions from energy loss models, where the difference between the R_{AA} of D and B mesons arises from the different masses of c and b quarks.

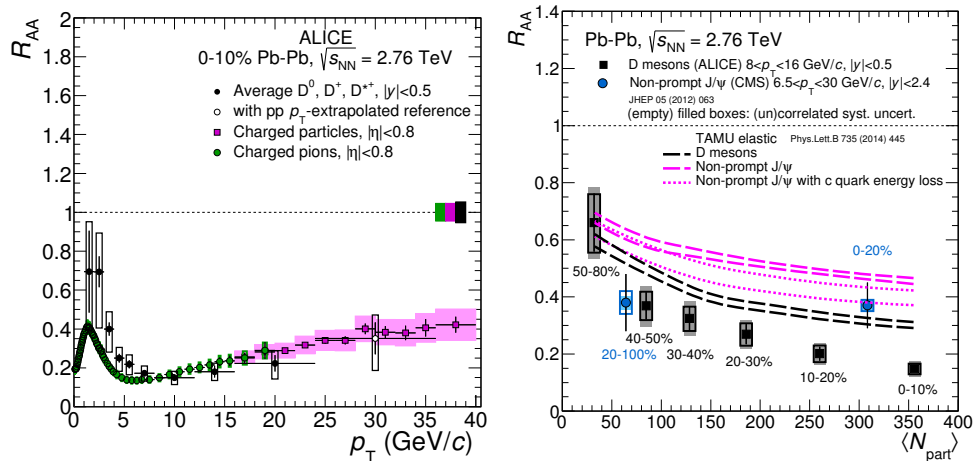


Figure 5. (Color online). D meson nuclear modification factor, R_{AA} , in Pb-Pb collisions at $\sqrt{s_{NN}} = 2.76 \text{ TeV}$. Left: R_{AA} as a function of p_T compared to charged hadrons and pions. Right: R_{AA} as a function of N_{part} [43] compared to non-prompt J/ψ measured by the CMS collaboration [44].

The v_2 of prompt D^0, D^+ and D^{*+} mesons at mid-rapidity was measured in three centrality classes: 0-10%, 10-30% and 30-50% [47, 48]. The comparisons of the D meson v_2 as a function of p_T with analogous results for inclusive charged particles are shown in Fig. 6. The v_2 decreases from peripheral to central collisions as expected due to the decreasing initial geometrical anisotropy. The average of the v_2 of D^0, D^+ and D^{*+} in the centrality class 30-50% is larger than zero with 5σ significance in the range $2 < p_T < 6 \text{ GeV}/c$. A positive v_2 is also observed for $p_T > 6 \text{ GeV}/c$, which most likely originates from the path length dependence of the in-medium partonic energy loss, although the present statistics does not allow to reach a firm conclusion on this. The measured D meson v_2 is comparable in magnitude with that of the charged particles, which are mostly light-flavour hadrons. This result indicates that low- p_T charm quarks take part in the collective motion of the system.

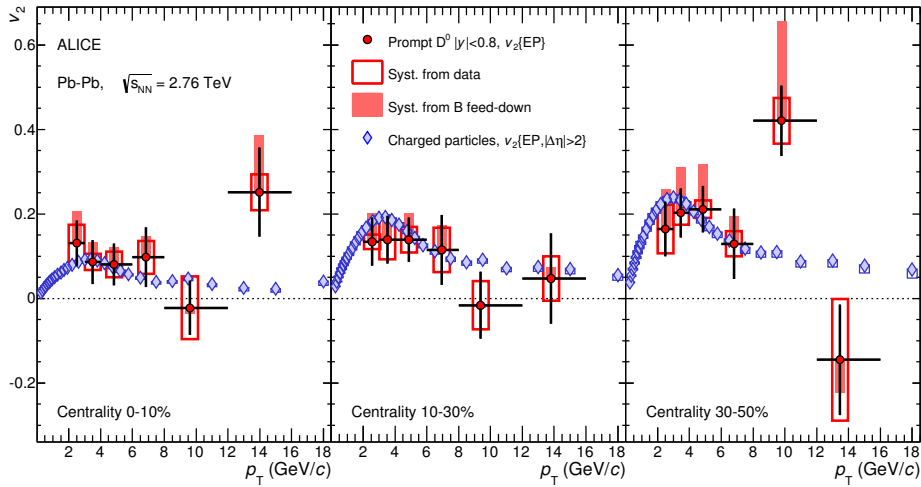


Figure 6. (Color online). D^0 meson v_2 as a function of p_T in three centrality ranges and compared with the v_2 of charged particles [47, 48].

R_{AA} and v_2 are two complementary measurements that can be used to better understand the connection between transport coefficients and the description of the in-medium energy loss [49].

3.4. Fluid-like behavior in small systems: pp and p-Pb collisions

The study of particle production in high-multiplicity pp and p-Pb collisions at the LHC has revealed unexpected new collective-like phenomena. The understanding of the phenomena is ongoing and different explanations have been proposed [50, 51, 52, 53, 54].

The CMS Collaboration studied the two-particle angular correlations of charged particles in pp collisions at $\sqrt{s} = 7$ TeV and discovered the ridge structure in small systems [55]. While the p_T -integrated correlation does not show any special feature, in the p_T range 1–3 GeV/c the near side long range angular correlation is clearly observed. Similar structures were also observed in p-Pb collisions at $\sqrt{s_{NN}} = 5.02$ TeV [56, 57, 58]. Furthermore, in high multiplicity events, non-zero second-order Fourier coefficients were extracted from the long-range correlations. Using the ALICE capabilities for particle identification, the proton v_2 was observed to be smaller than that for pions, up to about $p_T = 2$ GeV/c [59]. This effect is similar to the mass ordering of v_2 observed in heavy-ion collisions.

The transverse momentum spectra of charged pions, kaons and (anti)protons as a function of the event multiplicity have been measured up to 20 GeV/c [60]. At low p_T (< 2 –3 GeV/c) the spectra exhibit a hardening with increasing multiplicity, this effect is more important for heavy particles than for light particles. We are therefore observing features which resemble the radial flow effects well known from heavy-ion collisions [22] and which are well described when a hydrodynamical evolution of the system is considered. At the LHC [61] it was shown that for high multiplicity p-Pb events, the p_T spectra were described by the blast-wave function. Using the parameters obtained from the simultaneous fit to pion, kaon, proton and lambda p_T spectra the model is able to describe the multi-strange baryon p_T distributions ($p_T < 4$ GeV/c) [62]. The feature is also observed in pp collisions simulated with PYTHIA 8 [63, 64], where no hydrodynamical evolution is included, instead multiple partonic interactions (MPI) and color reconnection are producing the effects. Some ideas have been proposed to understand the role of MPI in data [65, 66, 67, 68, 69]. The multiplicity dependence of the intermediate to high- p_T particle production is studied with the particle ratios [60]. The proton-to-pion ratio

as a function of the event multiplicity exhibits a maximum (bump) at $p_T \approx 3 \text{ GeV}/c$ and the size of the bump increases with increasing multiplicity. On the other hand, at higher transverse momenta ($p_T > 10 \text{ GeV}/c$) the ratios return to the values measured for pp and Pb–Pb collisions. Any particle species dependence of the nuclear modification factor is therefore excluded.

In order to look for the presence of re-scattering effects in high multiplicity p–Pb collisions; the K^{*0} and ϕ relative to charged kaons production is studied as a function of the cube root of the average mid-rapidity charged particle density. In heavy-ion collisions the decreasing trend of K^{*0}/K with increasing fireball size has been explained as a consequence of a re-scattering of K^{*0} decay daughters in the hadronic phase. It is worth noticing that a similar trend is also observed in p–Pb collisions [70].

Finally, we discuss the latest results on multiplicity-dependent enhancement of strange and multi-strange hadron production in pp and p–Pb collisions [71]. Figure 7 shows a significant enhancement of strange to non-strange hadron production with increasing particle multiplicity in pp collisions. The behaviour observed in pp collisions resembles that of p–Pb collisions at a slightly lower centre-of-mass energy [62], both in the values of the ratios and in their evolution with the event activity. This suggests that the origin of strangeness production in hadronic collisions is driven by the characteristics of the event activity rather than by the initial-state collision system or energy. In the context of heavy-ion collisions, this effect (strangeness enhancement) has been considered a signature of the QGP formation. Recently, it has been pointed out that a perfect scaling of the particle ratios with the energy density holds for the different colliding systems [72] opening new possibilities for a better understanding of the QGP-like features in small systems.

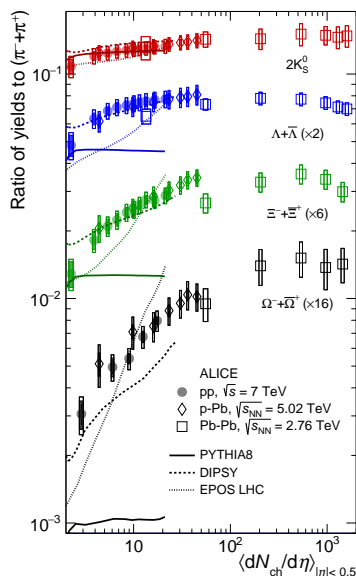


Figure 7. (Color online). Multiplicity dependence of strange and multi-strange hadrons yields normalized to that for charged pions. The empty and dark-shaded boxes show the total systematic uncertainty and the contribution uncorrelated across multiplicity bins, respectively. The values are compared to calculations from MC models and to results obtained in Pb–Pb and p–Pb collisions at the LHC.

4. Cosmic ray physics

Cosmic ray muons are created in Extensive Air Showers (EAS) following the interaction of cosmic ray primaries (protons and heavier nuclei) with nuclei in the upper atmosphere. Primary

cosmic rays span a broad energy range, starting at approximately 10^9 eV and extending to more than 10^{20} eV. The use of high-energy physics detectors for cosmic ray physics was pioneered by ALEPH [73], DELPHI [74] and L3 [75] during the Large Electron-Positron (LEP) collider era at CERN. An extension of these earlier studies is now possible at the LHC, where experiments can operate under stable conditions for many years.

ALICE has also been used to perform studies that are of relevance to astroparticle physics [76]. Recent studies focus on events containing more than four reconstructed muons in the ALICE TPC, which we refer to as multi-muon events, stem from primaries with energy $E > 10^{14}$ eV. ALICE dedicated 30.8 days of cosmic ray data taking recording approximately 22.6 million events containing at least one reconstructed muon. ALICE has reported (see Fig. 8) 5 events with, $N_\mu > 100$ and zenith angles less than 50° (corresponding to an area density $\rho_\mu > 5.9 m^2$ in a rate of 1.9×10^{-6} Hz).

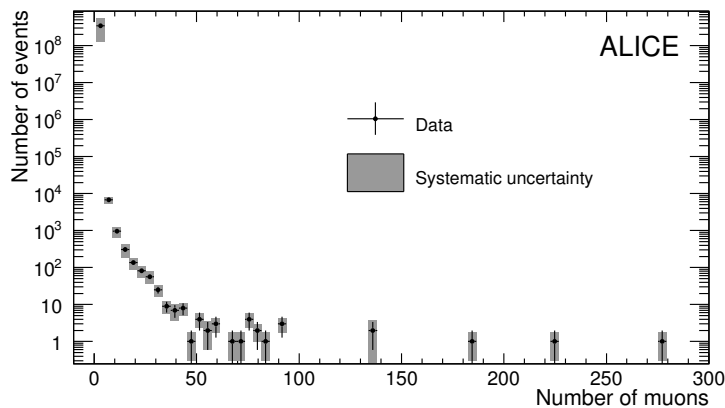


Figure 8. (Color online). Muon multiplicity distribution of the whole sample of data (2010-2013) corresponding to 30.8 days of data taking.

Figure 9 shows a comparison between data and MC simulations, the result suggests a mixed-ion primary cosmic ray composition with an average mass that increases with energy.

The ALICE measurement agrees with results from other experiments which work at the same energy domain (knee). Following the successful description of the magnitude of the muon multiplicity distribution (MMD) in the low-to-intermediate range of muon multiplicities the same simulation framework was used to study the frequency of high muon multiplicity (HMM) events.

It has been found that the observed rate of HMM events is consistent with the rate predicted by CORSIKA 7350 using QGSJET II-04 to model the development of the resulting airshower, assuming a pure iron composition for the primary cosmic rays.

Only primary cosmic rays with an energy $E > 10^{16}$ eV were found to give rise to HMM events. The expected rate of HMM events is sensitive to assumptions made about the dominant hadronic production mechanisms in air shower development. The latest version of QGSJET differs from earlier versions in its treatment of forward neutral meson production resulting in a higher muon yield and has been retuned taking into account early LHC results on hadron production in 7 TeV proton-proton collisions. This is the first time that the rate of HMM events, observed at the relatively shallow depth of ALICE, has been satisfactorily reproduced using a conventional hadronic model for the description of extensive air showers; an observation that places significant constraints on alternative, more exotic production mechanisms [76].

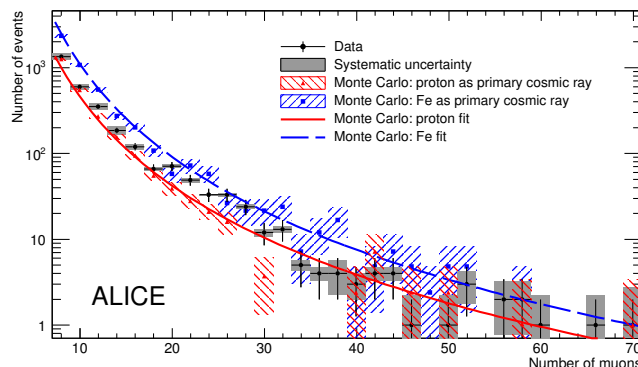


Figure 9. (Color online). The measured MMD compared with the values and fits obtained from CORSIKA simulations with proton and iron primary cosmic rays for 30.8 days of data taking. The errors are shown separately (statistical and systematic) for data, while for Monte Carlo they are the quadrature sum of the statistical and systematic uncertainties.

5. Outlook

In this paper we have presented the status and some highlights of the ALICE-LHC experiment, including the latest news on cosmic ray physics and the progress on the characterization of the hot and dense QCD medium created in the heavy-ion collisions. We have discussed several hot topics as the collective-like phenomena in small collision systems. More differential studies are needed in order to reveal the origin of the effects and their impact in our current understanding on the physics of heavy-ion collisions.

Acknowledgements

Support for this work has been received from CONACYT under the grant No. 260440 and grant No. 241408; from DGAPA-UNAM under PAPIIT grant IA102515.

References

- [1] ALICE Collaboration (B. Alessandro *et al.*), *Jour. of Phys. G: Nucl. and Part. Phys.* **32** (2006) 1295.
- [2] STAR Collaboration (J. Adams *et al.*), *Nucl. Phys.* **A757** (2005) 102.
- [3] PHOBOS Collaboration (B. B. Back *et al.*), *Nucl. Phys.* **A757** (2005) 28.
- [4] BRAHMS Collaboration (I. Arsene *et al.*), *Nucl. Phys.* **A757** (2005) 1.
- [5] PHENIX Collaboration Collaboration (K. Adcox *et al.*), *Nucl. Phys.* **A757** (2005) 184.
- [6] R. Bala, I. Bautista, J. Bielcikova and A. Ortiz, *Int. J. Mod. Phys.* **E25** (2016) 1642006, [arXiv:1605.03939 \[hep-ex\]](#).
- [7] ALICE Collaboration (B. B. Abelev *et al.*), *Int. J. Mod. Phys.* **A29** (2014) 1430044, [arXiv:1402.4476 \[nucl-ex\]](#).
- [8] A. Fernandez Tellez, ACORDE, The ALICE Cosmic Ray Detector, in *Proceedings, 30th International Cosmic Ray Conference (ICRC 2007): Merida, Yucatan, Mexico, July 3-11, 2007*, (2007), pp. 1201–1204.
- [9] ALICE Collaboration (J. Adam *et al.*), *Phys. Lett.* **B754** (2016) 235.
- [10] PHENIX Collaboration (A. Adare *et al.*), *Phys. Rev.* **C91** (2015) 064904.
- [11] A. Ayala *et al.*, *Nucl. Phys.* **B897** (2015) 77.
- [12] ALICE Collaboration (K. Aamodt *et al.*), *Phys. Rev. Lett.* **106** (2011) 032301.
- [13] M. Floris, *Nucl. Phys.* **A931** (2014) 103.
- [14] ALICE Collaboration (K. Aamodt *et al.*), *Phys. Lett.* **B696** (2011) 328.
- [15] ALICE Collaboration (B. Abelev *et al.*), *Phys. Rev.* **C91** (2015) 024609.
- [16] R. Hanbury Brown *et al.*, *Nature* **178** (1956) 1046.
- [17] R. J. Fries *et al.*, *Ann. Rev. Nucl. Part. Sci.* **58** (2008) 177.

- [18] S. Sapeta *et al.*, *Eur. Phys. J.* **C55** (2008) 293.
- [19] R. Bellwied *et al.*, *Phys. Lett.* **B691** (2010) 208.
- [20] ALICE Collaboration (B. Abelev *et al.*), *Phys. Rev.* **C88** (2013) 044910.
- [21] ALICE Collaboration (B. Abelev *et al.*), *Phys. Lett.* **B736** (2014) 196.
- [22] ALICE Collaboration (J. Adam *et al.*), *Phys. Rev.* **C93** (2016) 034913.
- [23] P. Bozek *et al.*, *Phys. Rev.* **C85** (2012) 064915.
- [24] I. A. Karpenko *et al.*, *Phys. Rev.* **C87** (2013) 024914.
- [25] K. Werner *et al.*, *Phys. Rev.* **C85** (2012) 064907.
- [26] C. Shen *et al.*, *Phys. Rev.* **C84** (2011) 044903.
- [27] A. Ortiz, *Nucl. Phys.* **A943** (2015) 9.
- [28] E. Schnedermann *et al.*, *Phys. Rev.* **C48** (Nov 1993) 2462.
- [29] ALICE Collaboration (B. Abelev *et al.*), *JHEP* **06** (2015) 190.
- [30] ALICE Collaboration (B. Abelev *et al.*), *Phys. Rev.* **C88** (2013) 044909, [arXiv:1301.4361 \[nucl-ex\]](#).
- [31] ALICE Collaboration (B. Abelev *et al.*), *Phys. Lett.* **B722** (2013) 262.
- [32] ALICE Collaboration (J. Adam *et al.*), *Phys. Lett.* **B753** (2016) 511.
- [33] ALICE Collaboration (J. Adam *et al.*), *JHEP* **09** (2015) 170.
- [34] ALICE Collaboration (K. Aamodt *et al.*), *Phys. Rev. Lett.* **108** (2012) 092301.
- [35] ALICE Collaboration (J. Adam *et al.*), *Phys. Lett.* **B746** (2015) 1.
- [36] ATLAS Collaboration (G. Aad *et al.*), *Phys. Rev. Lett.* **111** (2013) 152301.
- [37] ALICE Collaboration (B. Abelev *et al.*), *Phys. Lett.* **B719** (2013) 18.
- [38] CMS Collaboration (S. Chatrchyan *et al.*), *Phys. Rev. Lett.* **109** (2012) 022301.
- [39] ALICE Collaboration (J. Adam *et al.*), *JHEP* **03** (2016) 081.
- [40] ALICE Collaboration (J. Adam *et al.*), *JHEP* **03** (2016) 082.
- [41] ALICE Collaboration (B. Abelev *et al.*), *Phys. Rev. Lett.* **109** (2012) 112301.
- [42] M. Djordjevic, *Phys. Rev. Lett.* **112** (2014) 042302.
- [43] ALICE Collaboration (J. Adam *et al.*), *JHEP* **11** (2015) 205.
- [44] CMS Collaboration (S. Chatrchyan *et al.*), *JHEP* **05** (2012) 063.
- [45] A. Andronic *et al.*, *Eur. Phys. J.* **C76** (2016) 107.
- [46] M. Nahrgang *et al.*, *Phys. Rev.* **C89** (2014) 014905.
- [47] ALICE Collaboration (B. Abelev *et al.*), *Phys. Rev. Lett.* **111** (2013) 102301.
- [48] ALICE Collaboration (B. Abelev *et al.*), *Phys. Rev.* **C90** (2014) 034904.
- [49] A. Ayala, I. Dominguez, J. Jalilian-Marian and M. E. Tejeda-Yeomans (2016) [arXiv:1603.09296 \[hep-ph\]](#).
- [50] L. J. Gutay *et al.*, *Int. J. Mod. Phys.* **E24** (2015) 1550101.
- [51] I. Bautista *et al.*, *Phys. Rev.* **D92** (2015) 071504.
- [52] K. Dusling *et al.*, *Phys. Rev. Lett.* **108** (2012) 262001.
- [53] K. Dusling *et al.*, *Phys. Rev.* **D87** (2013) 051502.
- [54] K. Dusling *et al.*, *Phys. Rev.* **D93** (2016) 014034.
- [55] CMS Collaboration (V. Khachatryan *et al.*), *JHEP* **09** (2010) 091.
- [56] CMS Collaboration (S. Chatrchyan *et al.*), *Phys. Lett.* **B718** (2013) 795.
- [57] ALICE Collaboration (B. Abelev *et al.*), *Phys. Lett.* **B719** (2013) 29.
- [58] ATLAS Collaboration (G. Aad *et al.*), *Phys. Rev. Lett.* **110** (2013) 182302.
- [59] ALICE Collaboration (B. Abelev *et al.*), *Phys. Lett.* **B726** (2013) 164.
- [60] ALICE Collaboration (J. Adam *et al.*), *Phys. Lett.* **B760** (2016) 720, [arXiv:1601.03658 \[nucl-ex\]](#).
- [61] ALICE Collaboration (B. Abelev *et al.*), *Phys. Lett.* **B728** (2014) 25.
- [62] ALICE Collaboration (J. Adam *et al.*) (2015) [arXiv:1512.07227 \[nucl-ex\]](#).
- [63] R. Corke *et al.*, *JHEP* **03** (2011) 032.
- [64] A. Ortiz *et al.*, *Phys. Rev. Lett.* **111** (2013) 042001.
- [65] ALICE Collaboration (B. Abelev *et al.*), *JHEP* **09** (2013) 049.
- [66] ALICE Collaboration (B. Abelev *et al.*), *Phys. Lett.* **B741** (2015) 38.
- [67] ALICE Collaboration (B. Abelev *et al.*), *Eur. Phys. J.* **C72** (2012) 2124.
- [68] A. Ortiz *et al.*, *Nucl. Phys.* **A941** (2015) 78.
- [69] A. Ortiz, G. Bencedi and H. Bello (2016) [arXiv:1608.04784 \[hep-ph\]](#).
- [70] ALICE Collaboration (J. Adam *et al.*), *Eur. Phys. J.* **C76** (2016) 245, [arXiv:1601.07868 \[nucl-ex\]](#).
- [71] ALICE Collaboration (J. Adam *et al.*) (2016) [arXiv:1606.07424 \[nucl-ex\]](#).
- [72] Cuautle, E. and Paić, G. (2016) [arXiv:1608.02101 \[hep-ph\]](#).
- [73] C. Grupen *et al.*, *Nucl. Instrum. Meth.* **A510** (2003) 190.
- [74] DELPHI Collaboration (J. Ridky and P. Travnicek), *Nucl. Phys. Proc. Suppl.* **138** (2005) 295, [,295(2005)].
- [75] L3 Collaboration (P. Ladron de Guevara), *Nucl. Phys. Proc. Suppl.* **143** (2005) 500.
- [76] ALICE Collaboration (J. Adam *et al.*), *JCAP* **1601** (2016) 032, [arXiv:1507.07577 \[astro-ph.HE\]](#).